Image charge effects on colloidal crystal ordering

Shalabh Tandon, R. Kesavamoorthy,[a),b)] and Sanford A. Asher[b)]
Department of Chemistry, Materials Research Center, University of Pittsburgh, Pittsburgh, Pennsylvania 15260

(Received 18 November 1996; accepted 15 July 1998)

We theoretically investigated the effect of the container wall on the structural ordering of aqueous dispersions of negatively charged electrostatically stabilized colloidal spherical particles. The colloidal crystal contained between two quartz plates is modeled as a set of crystal planes oriented parallel to the quartz walls. We consider the electrostatic interactions between the particles and the container wall, and the particles and their induced image charges. The position-dependent interaction energies of a plane with its neighbors and the induced image charges are calculated under the Debye–Hückel approximation. We also theoretically investigate the effect of charged container walls on the ordering of the colloidal particle dispersion. For zero wall surface charge, the colloidal sphere plane nearest to the container wall is held in a deeper potential well than are interior colloidal planes. A negative wall surface charge creates a shallower well for the nearest colloidal sphere plane, which is still deeper than that of the interior planes. A positive wall surface charge creates the deepest potential well. These results rationalize our recent observations of the initial nucleation of crystalline colloidal array by formation of 2D hexagonal colloidal layers near the container wall. We calculate the root-mean-square displacement of the planes at various distances from the wall and use the Lindermann-type melting criteria to examine ordering. [S0021-9606(98)51139-7]

I. INTRODUCTION

Aqueous dispersions of polystyrene colloidal particles show gas, liquid, glass, and crystalline phases similar to atomic and molecular systems depending on the particle concentration n_p, impurity concentration n_i, particle charge Ze, temperature T, particle diameter $2a$, and the medium dielectric constant ϵ.[1–5] Colloidal particles acquire a net charge when dispersed in water due to the ionization of the surface functional groups.[1] The particles are surrounded by diffuse ion clouds extending from the particle surface into the solution. The interparticle interaction is fairly well represented by a screened Coulomb repulsion extending over many particle diameters.[6] To minimize the interparticle repulsive interactions, colloidal particles self-assemble into ordered arrays and can crystallize into body-centered-cubic (bcc) or face-centered-cubic (fcc) structures. Bcc (fcc) is thermodynamically favored for dilute (concentrated) suspensions.[1,7–10] Highly efficient optical filters, which utilize single crystals of these arrays to Bragg diffract narrow bandwidths of radiation, have been developed.[11]

The ionic strength dependence of structural ordering of colloidal dispersions has been investigated previously.[4,12–14] At high n_i values, the dispersion is disordered (gaslike), and as n_i is reduced, the particle concentration near the wall increases,[12,13] causing two-dimensional (2-D) hexagonal layers of particles to nucleate parallel to the wall, while away from the wall the dispersion exhibits either gaslike disorder or liquidlike order.[13,15] As n_i is reduced further, the 2D layers near the wall crystallize into a three-dimensional (3D) bcc (fcc) crystal with the (110) planes [(111) planes] parallel to the wall, even though the bulk shows a 2D layered structure.[13,14] Finally, at low n_i, the whole dispersion exhibits a 3D crystal structure.[14,16] The hexagonal 2D planes are known to nucleate first near the wall during crystallization, and disorder last during melting of the colloidal crystal.[12–14] Although Kesavamoorthy *et al.*[12,14,17] conjectured that the interaction of the colloidal particles with their induced image charges in the dielectric (container wall) is responsible for the observed increased structural ordering near the wall, this possibility has not yet been experimentally or theoretically investigated. Grier and Murray[18] investigated the dynamics of freezing of supercooled colloidal suspensions contained between two parallel glass plates using optical microscopy. Their investigations revealed the gradual increase of the colloidal particle concentration near the glass wall as the order develops, and the development of hexagonal ordering in the plane nearest to the wall. The nearest plane was shown to vibrate asymmetrically about its equilibrium position with a smaller amplitude toward the wall than away from the wall. During crystallization the nearest plane orders first. Subsequently, the second nearest plane orders, followed by the third, fourth, until the whole suspension orders into a colloidal crystalline array. In their investigation of colloidal hard-sphere glasses formed by centrifugal quenching of hard-sphere colloidal liquids, van Blaaderen and Wiltzius[19] reported that a wall-induced layering was observed close to the wall to a distance of ~10 layers.

In the present work, we investigate theoretically the effect of the container wall on the structural ordering of nega-

[a)]Permanent address: Materials Science Division, Indira Gandhi Center for Atomic Research, Kalpakkam 603 102 India.
[b)]Authors to whom correspondence should be addressed.

tively charged colloidal dispersions. We modeled the colloidal crystal as a set of planes parallel to the wall which have a uniform surface charge density, σ, and a thickness identical to the particle diameter, $2a$. The surface charge density on the plane is calculated from the sphere surface charge, the number of spheres in the plane, and the concentration of small ions (counter ions and impurity ions) present within the plane. The electrostatic interactions with the container wall is assumed to derive from the wall surface charge and induced image charges in the dielectric. Under the Debye–Hückel approximation, the potential energy (PE) as a function of the distance of a plane from the wall is calculated, considering plane–plane interactions and plane–image charge interactions. Using the PE curve, we obtain the root-mean-square (rms) displacement of the plane around its equilibrium position and compare the rms values of planes near the wall to those far away from the wall. The rms value of the plane estimated from the computer simulation of the colloidal crystal melting[4,20] is compared with the present value. Based on the present calculations, we explain the recent observations of 2-D hexagonal layers near the wall and we find a greater stability of the plane nearest to the wall as compared to interior planes. Positive charge on the wall stabilizes and negative charge destabilizes these two-dimensional colloid sphere planes.

II. MODELING

In the present investigation, the colloidal crystal is considered to be confined between two widely separated smooth quartz plate walls.[13,16,18] In this parallel plate geometry, the colloidal crystal is modeled as a set of planes of thickness identical to the particle diameter oriented parallel to the quartz plates.[16,21,22] These would be the (110) planes for a bcc structure or the (111) planes for an fcc structure. The average interplanar separation is determined by the average particle concentration and the crystal structure. The plane is considered to be vibrating in one dimension (normal to itself) at a temperature T, with a thermal energy of $(1/2)Nk_BT/\mathrm{cm}^2$, where N is the number of particles/cm^2 in the plane and k_B is the Boltzmann constant. The plane thickness, $2a$, is considered constant during the plane vibration. The charge density on the plane is uniform and is determined as described below.

A. Charge density in the plane, σ

The plane consists of negatively charged colloidal particles and small ions (counterions and impurity ions). The small ion concentration around a particle is calculated using Debye–Hückel (D–H) approximation with a renormalized particle charge.[15,16,23,24]

The small ion net charge density at a distance r from a particle center is given by[6]

$$C(r)=\frac{-2n_oe^2\psi(r)}{k_BT}, \tag{1}$$

where e is the electronic charge and $2n_o$ is the average total small ion concentration (assumed to be monovalent) given by

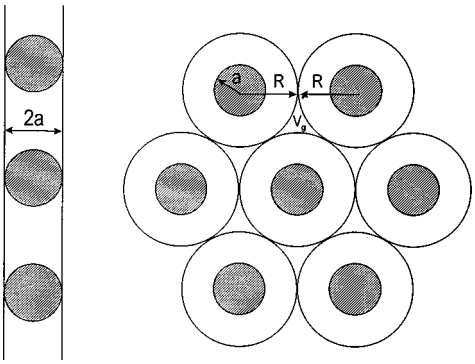

FIG. 1. Schematic representation of a colloidal particle plane: (a) Side view of the plane; (b) front view of the plane, where $2R$ is the interparticle distance, a is the particle radius, and V_g is the gap volume.

$$2n_o=n_pZ+n_i, \tag{2}$$

where Z is the reduced particle charge number, n_pZ is the counterion concentration, and n_i is the total impurity ion concentration. The screened Coulomb potential at r is given by

$$\psi(r)=\frac{-Ze}{\epsilon}\left(\frac{e^{\kappa a}}{1+\kappa a}\right)\frac{e^{-\kappa r}}{r}, \tag{3}$$

where a is the particle radius, ϵ is the medium dielectric constant, and κ is the inverse Debye screening length given by

$$\kappa^2=\frac{8\pi e^2n_o}{\epsilon k_BT}. \tag{4}$$

In order to determine the small ion charge confined in the plane, a circular cylindrical cell of thickness $2a$ and radius R is constructed around each particle ($2R$ is the average interparticle separation distance in the plane) as shown in Fig. 1. The small ion net charge around a particle in the cell is given by

$$C_1=2\int_{z=0}^{a}\int_{\rho=\sqrt{a^2-z^2}}^{R}2\pi\rho d\rho C(r)dz, \tag{5}$$

where $r^2=\rho^2+z^2$. Substituting Eqs. (1)–(4) in (5) and carrying out the integration,

$$C_1=\frac{Ze\kappa}{(1+\kappa a)}\left[a-e^{\kappa a}\int_0^a e^{-\kappa\sqrt{(z^2-R^2)}}dz\right]. \tag{6}$$

Equation (6) can be approximated as

$$C_1=\frac{Ze\kappa a}{(1+\kappa a)}\left[1-\exp\left(-\kappa\left(\sqrt{R^2+\frac{a^2}{2}}-a\right)\right)\right]. \tag{7}$$

The circular cylindrical cells do not completely fill the plane and a gap exists between the cells, as shown in Fig. 1. The gap volume, V_g, is given as

$$V_g=(2\sqrt{3}R^2-\pi R^2)a. \tag{8}$$

The small-ion charge in V_g is approximated as

$$C_2=V_gC(R)=\frac{Ze\kappa^2Ra}{4\pi(1+\kappa a)}(2\sqrt{3}-\pi)e^{-\kappa(R-a)}. \tag{9}$$

The net charge in the plane per cm^2 area is

$$\sigma=(-Ze+C_1+2C_2)N. \tag{10}$$

In Eq. (10), C_2 is multiplied by 2 since each particle gives rise to two gap volumes. Thus, small ions contained in the colloidal sphere plane lower the magnitude of σ below the value ZeN.

In this work, we modeled the charge distribution in the colloidal sphere plane to be uniform. In fact, the plane contains negatively charged colloidal spheres self-assembled in a 2-D array and its accompanying cloud of small ions, impurity ions, and the counterions. The region between the colloidal sphere planes contains only ion clouds. The charge distribution in the colloidal sphere planes shows the two-dimensional periodicity of the hexagonally distributed particles. The double layer forces and the interaction free energy between two heterogeneously charged surfaces have been worked out recently.[25,26] However, for the sake of simplicity, we model the colloidal sphere planes to be homogeneously charged with an effective negative charge density, σ, given by Eq. (10).

B. The interplanar interaction

The planes are considered to interact electrostatically only with nearest neighbor planes. The screened Coulomb interaction energies between two slabs having a charge density per unit area of σ, with a plane thickness $2a$, and the interplanar center to center distance s, is given under D–H approximation as[6]

$$U_1(s)=\frac{2\pi\sigma^2}{\epsilon\kappa}\,e^{-\kappa(s-2a)}. \tag{11}$$

This equation can also be derived by considering the interaction free energy between two surfaces having a periodic charge modulation.[25] The free energy expression of Miklavic *et al.*[25] for two surfaces with a charge modulation can be approximated by our colloid particle planes of average uniform surface charge density without a periodic charge modulation. Their expression reduces to Eq. (11), but with a constant 8 instead of 2. This difference occurs because the charge compensating counterions are present on only one side of the charged surface in their model, whereas they are present on both sides of our colloidal planes of thickness $2a$. Equation (11) is valid in cases of a thick double layer, $ka<3$, which is the case considered here (*vide infra*). In addition, Eq. (11) is valid for the case of constant surface potential as well as for the case of constant surface charge.

C. The interaction between a plane and its image

Consider a charge in a medium placed near the boundary between media 1 and 2 which have different dielectric constants. This charge polarizes the second medium and electrostatically interacts with this induced polarization. The interaction energy can be obtained by calculating the induced image charge. The charge q placed in water (medium 1, $\epsilon=78$) at a distance r from the water–quartz boundary induces an image charge q_i in quartz (medium 2, $\epsilon'=4.1$) at the same distance from the boundary. q_i is given by[27,28]

$$q_i=\frac{\epsilon-\epsilon'}{\epsilon+\epsilon'}\,q. \tag{12}$$

Hence, a plane of thickness $2a$ and surface charge density σ at a distance $(D+a)$ from the wall to the plane center induces an image plane of thickness $2a$ and surface charge density σ_i at a distance $(D+a)$ inside the quartz dielectric. The interaction between the plane and its image is given by

$$U_{ip}(2D)=\frac{2\pi\sigma\sigma_i}{\epsilon\kappa}\,e^{-2\kappa D}, \tag{13}$$

where $2D$ is the surface to surface distance between the plane and its image. σ_i is obtained from σ using Eq. (12), and for the case of colloidal dispersion confined between quartz plates, both σ and σ_i are negative.

D. Interaction between the plane and the wall

Let σ_w be the surface charge density of the wall (interface between the dispersion and quartz). The small ions, present in the dispersion, screen the wall charge. The plane having a surface charge density σ interacts with the wall, and the interaction energy U_w is given by

$$U_w(D)=\frac{4\pi\sigma\sigma_w}{\epsilon\kappa}\,e^{-\kappa D}, \tag{14}$$

where D is the distance between the wall and the plane surface. If σ and σ_w are of the same sign, U_w is positive, otherwise it is negative. A clean quartz surface is negatively charged in water due to the presence of surface silanol groups, and thus it interacts repulsively with the negatively charged colloidal plane. Equation (14) contains the factor 4 instead of 2, since the charge compensating counterions are present on both sides of the colloidal plane but on only one side of the container wall surface.

The concentration of silanol groups on the quartz surface is pH dependent.[29] Therefore, if the pH of the dispersion is known, a fairly accurate zeta potential of the quartz wall can be obtained.[29] Assuming that the zeta potential and the effective surface potential are identical, the surface charge density at the wall can be obtained using[6]

$$\sigma_w=\frac{\epsilon\kappa\psi_w}{4\pi}, \tag{15}$$

where ψ_w is the surface potential of the quartz wall. If the quartz surface were functionalized with ionizing species, the wall charge could also have a net positive surface charge density $(\sigma_w>0)$ or even a zero surface charge density (neutral, $\sigma_w=0$).

E. Interaction between the plane and the image charges induced by the wall screening ions

The charge on the quartz wall is screened by the small ions in the dispersion with an inverse screening length, κ. This small ion distribution near the wall, $\rho(r)$, (r is the distance from the wall) induces an image charge distribution in the quartz dielectric. The induced image charge distribution, $\rho_i(r')$, (where r' is the distance of the image charge from

the wall, $r'=r$), also has the same inverse screening length. $\rho_i(r')$ is calculated using Eq. (12),[27,28] where $\rho(r)$ is given as[6]

$$\rho(r)=\frac{-2n_o e^2\psi_w}{k_B T}\, e^{-\kappa r}. \tag{16}$$

The interaction energy between the colloid plane nearest to the wall and the screening ion image charge distribution $\rho_i(r')$ is given by

$$U_i(D)=\int_{r'=0}^{\infty}\rho_i(r')\psi_p(D+r')dr', \tag{17}$$

where D is the distance of the colloid plane surface from the wall and r' is the distance of the image charge from the wall. The potential due to the colloid plane at the location of the image charge is given by[6]

$$\psi_p(D+r')=\frac{2\pi\sigma}{\epsilon\kappa}\, e^{-\kappa(D+r')}. \tag{18}$$

For a negatively charged colloidal particle, U_i is negative for a negatively charged wall, positive for a positively charged wall, and zero for a neutral wall.

F. Potential energy curve

Using Eqs. (11), (13), (14), and (17), we obtain the potential energy (PE) curves for the first three planes nearest to the wall as a function of the distance from the wall. The interaction potential decreases exponentially with distance and hence the PE curves for the planes far from the wall are unaffected by either the image charges or the wall charges. The PE curve for the interior planes is obtained from Eq. (11). The second neighbor interaction of a plane is calculated to be about 10^5 times smaller than the first neighbor interaction and is therefore neglected. The PE curve of an interior plane j is obtained by spacing the neighboring planes $j-1$ and $j+1$ and at a distance $2d_{hkl}$. d_{hkl}, the average interlayer spacing, is determined from n_p and the crystal structure. The total potential energy, U_t, is calculated as a function of the center plane position

$$U_t(s)=U_1(s-2a)+U_1(2d_{hkl}-s-2a), \tag{19}$$

where s is the center to center distance between the plane j and its left neighbor, $j-1$.

The PE curve for the plane nearest to the wall (plane 1) is obtained by fixing the position of the second plane from the wall and varying the position of plane 1. The potential energy is calculated using

$$U_{t1}(s_1)=U_w(s_1-a)+U_{ip}(2s_1-2a)+U_i(s_1-a)+U_1(d_2-s_1-2a), \tag{20}$$

where s_1 and d_2 are the distances of the centers of planes 1 and 2 from the wall, respectively. For the PE curve of plane 2 (second nearest plane to the wall), the centers of planes 1 and 3 are fixed at d_1 and d_3 from the wall, while the distance between the wall and plane 2 center, s_2, is varied from d_1+2a to d_3-2a, and the potential energy is given as

TABLE I. Colloidal systems studied: crystal structure, particle concentration n_p, plane thickness $2a$, renormalized charge Z, melting impurity concentration n_i^m, the Lindemann-type parameter W_p, calculated here for the interior colloid plane, and the effective charge density of the plane σ.

System	Crystal structure	$n_p/10^{13}$ cm^3	$2a$ /nm	Z	n_i^m/n_pZ	$-\sigma$ statcoul/cm^2	W_p %
A	fcc	8.0	83	600	1.03	233.6	4.78
B	fcc	16.0	83	1150	0.94	460.0	4.61
C	bcc	8.0	83	1150	0.72	367.7	4.07
D	bcc	0.42	109	600	1.19	50.2	4.44

$$U_{t2}(s_2)=U_w(s_2-a)+U_{ip}(d_1+s_2-2a)+U_i(s_2-a)+U_1(s_2-d_1-2a)+U_1(d_3-s_2-2a). \tag{21}$$

Similarly, the potential energy curve of plane 3 is given by

$$U_{t3}(s_3)=U_w(s_3-a)+U_{ip}(d_1+s_3-2a)+U_i(s_3-a)+U_1(s_3-d_2-2a)+U_1(d_4-s_3-2a), \tag{22}$$

where d_4 is the distance of the center of plane 4 from the wall and s_3 is the distance of the center of plane 3 from the wall.

The effects of the wall charge and image charge at distances as large as d_4 are negligible as compared to $U_1(d_{hkl}-2a)$. Hence, only the PE curves of planes 1, 2, and 3 are obtained using Eqs. (20), (21), and (22), respectively. We assume a set of values for d_1, d_2, and d_3 ($d_4=d_{hkl}$) and obtain the PE curves for planes 1, 2, and 3. The positions of the calculated potential minima are used as the new values for d_1, d_2, and d_3 to recalculate the PE curves and to converge on a final minimum PE position for planes 1, 2, and 3; the calculation converges to a unique set of equilibrium d values for planes in a stable structure.

G. Root-mean-square displacement of the plane, $\sqrt{\langle U_p^2\rangle}$, (rms)

The potential energy is calculated at a temperature, T ($=298$ °K). The plane is assumed to vibrate perpendicular to the wall in its potential well. The rms is obtained by calculating the plane displacements $\sqrt{\langle U_p^2\rangle}$ from the potential minimum position at an energy, $\Delta U=(1/2)Nk_BT$, above the PE minimum value; N is the average number of particles per unit area of the plane. Planes with smaller $\sqrt{\langle U_p^2\rangle}$ values vibrate less and are more rigidly fixed as compared to planes having larger $\sqrt{\langle U_p^2\rangle}$ value. We recently calculated the impurity concentrations needed for melting these crystals from Monte Carlo simulations.[19] We determine here the scaled rms displacement of the plane, $n_p^{1/3}\sqrt{\langle U_p^2\rangle}$, for different colloidal systems at their melting impurity concentrations, n_i^m. The scaled rms displacement of an interior plane at n_i^m is $W_{p\lambda}$, and those of first second and third planes near the wall are Δ_1, Δ_2, Δ_3.

III. RESULTS AND DISCUSSION

Table I lists the parameters for the four different colloidal crystals (2 fcc and 2 bcc crystals) studied here. These colloidal crystals were modeled to have sufficient impurity concentrations that the macroscopic colloidal crystals are

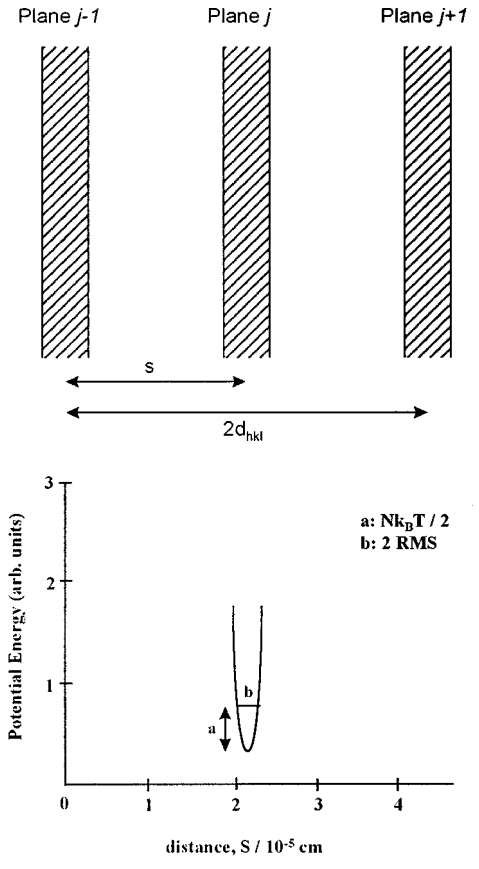

FIG. 2. Schematic representation of parallel colloid particle planes along with the potential energy curve for plane–plane interactions.

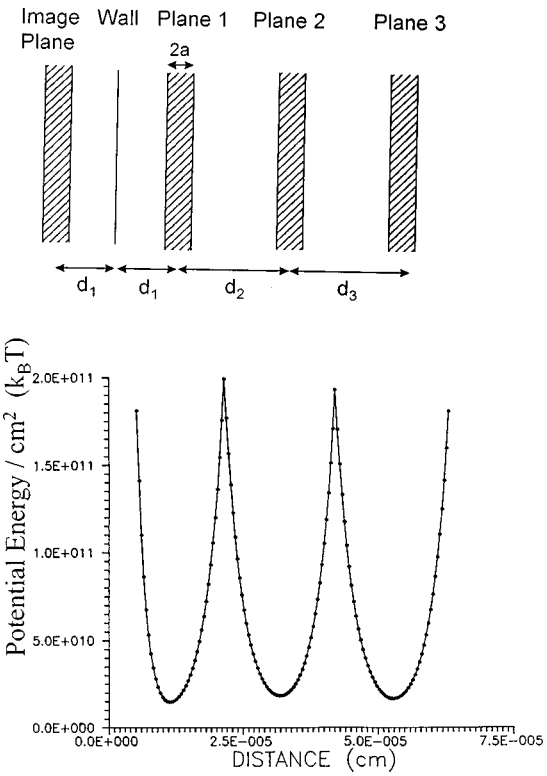

FIG. 3. Schematic representation of parallel particle planes, the container wall, and the image charge of the first particle plane. Also shown is the total potential energy curve.

calculated to be at their melting transition phase boundary at room temperature. These systems have been studied experimentally[16,30–32] and by Monte Carlo simulation.[4] Under the present model, an fcc (bcc) crystal is modeled as (111) planes [(110) planes] of particle thickness $2a$ which are oriented parallel to the quartz wall. Figure 1 shows the particle arrangement in (111) planes of an fcc crystal at 298 °K where the interparticle separation is $(4/n_p)^{1/3}/\sqrt{2}$. The average interparticle separation in the (110) plane of the bcc crystal is $(2/n_p)^{1/3}(1+\sqrt{3})/3$. The effective surface charge density on the plane, σ, is calculated from Eq. (10) and is given in Table I.

The wall and the image charges have no effect on the interior planes, therefore the PE curve for interior planes is obtained using Eq. (19). Figure 2 shows the positions of three interior planes and the PE curve for an interior plane. We calculate the Lindemann-type melting parameter, W_p, from the calculated PE curve by determining the rms value, $\sqrt{\langle U_p^2 \rangle}$, of a plane far from the wall from the positions at an energy of $(1/2)Nk_BT$ above the PE minimum and normalizing it by the length scale $(n_p^{-1/3})$. The W_p values calculated here for various colloidal crystals are given in Table I along with the melting impurity concentration, n_i^m. W_p found here is much lower than the Lindemann parameter, W, for these systems calculated previously,[4] where W is the rms displacement of a particle at melting of a colloidal crystal in length scale unit of $n_p^{-1/3}$.[2,33,34] W_p for both fcc crystals are larger than those for the bcc crystals, whereas W calculated previously were similar for all crystals at ~ 0.19 for the three-dimensional case.[4] Since W_p is defined for only one dimension, it should be related to $W/(\sqrt{3}) \approx 0.11$.

The reason for our lower calculated W_p is not yet clear. It is possible that we calculate too large an effective σ value. Our model assumes a rigid plane structure of thickness $2a$. However, the plane would be thicker if the particle vibrations were taken into account. This larger plane would encompass more of the small ions. This would reduce the σ value and increase the W_p toward 0.11.

A. Neutral wall, $\sigma_w = 0$

In the previous section we calculated W_p for interior colloid planes at the impurity ion concentration where the crystals should melt. The image charge does not affect the interior planes but influences planes near the wall. In this section we will consider the case when the container wall has zero surface charge density $(\sigma_w = 0)$ and has no electrostatic interactions with the colloid planes. In addition, $U_i(r) = 0$ due to the absence of the screening small ion cloud near the wall. However, plane 1 induces its image in the quartz wall and interacts with it, as well as with plane 2. Similarly, plane 2 is considered to interact with plane 1, plane 3, and the image of plane 1. Finally, plane 3 interacts with planes 2 and 4 and the image of plane 1. The PE curves for planes 1, 2, and 3 are calculated using Eqs. (20), (21), and (22), respectively, with both U_w and $U_i = 0$. Figure 3 shows the positions of planes 1, 2, and 3 with respect to the wall and the image plane along with the PE curves corresponding to planes 1, 2, and 3 for system A. The potential energy curve is asymmet-

TABLE II. Calculated parameters for the neutral wall.

System	A	B	C	D
n_i^m/n_pZ	1.03	0.94	0.72	1.19
$-\sigma$ (statcoul/cm^2)	233.60	460.00	367.70	50.20
σ_w	0.00	0.00	0.00	0.00
$N/10^9$ cm^2	1.702	2.7008	1.654	0.232
d_1/nm	111.50	88.00	109.00	312.00
d_2/nm	206.00	166.00	202.00	538.00
d_3/nm	208.30	168.00	204.00	547.00
d_{hkl}/nm	212.70	168.80	206.70	552.20
Δ_1 %	3.32	3.49	3.02	3.40
Δ_2 %	4.40	4.26	3.66	3.90
Δ_3 %	4.63	4.45	3.94	4.22
W_p %	4.78	4.61	4.07	4.44

TABLE III. Calculated parameters for the negative wall.

System	A	B	C	D
n_i^m/n_pZ	1.03	0.94	0.72	1.19
$-\sigma$ (statcoul/cm^2)	233.60	460.00	367.70	50.20
$-\sigma_w$ (statcoul/cm^2)	159.60	258.50	187.70	62.80
$N/10^9$ cm^2	1.702	2.7008	1.654	0.232
d_1/nm	163.00	120.00	160.00	582.00
d_2/nm	206.00	166.00	204.00	552.20
d_3/nm	208.30	168.00	206.00	552.20
d_{hkl}/nm	212.70	168.80	206.70	552.20
Δ_1 %	3.92	4.07	3.83	4.33
Δ_2 %	4.35	4.34	3.86	4.33
Δ_3 %	4.61	4.48	3.92	4.33
W_p %	4.78	4.61	4.07	4.44

ric where the repulsive interaction is steeper for the first plane on the side toward the quartz plate. This results from repulsion by the image charge. The potential well is slightly deeper for the first plane than the others. Using the PE results we can calculate scaled rms values for colloid planes near the wall, Δ_1, Δ_2, and Δ_3.

Table II gives the equilibrium positions of the planes 1, 2, and 3 along with their scaled rms values. It is observed that $\Delta_1<\Delta_2<\Delta_3<W_p$, implying that the nearest plane is held more rigidly as compared to the other planes. Plane 1 vibrates less than plane 2 and plane 2 less than plane 3. If we consider that a plane disorders completely (melts) when its Lindemann-type parameter reaches W_p, the first few planes will preserve their crystalline identity even after the interior planes melt. Thus, the first plane disorders last during crystal melting and orders first during crystallization. In addition, we observe from Table II that $d_1<d_2<d_3<d_{hkl}$, which means that the planes near to the wall are attracted toward the wall. This result indicates that the particle concentration near the wall is higher than within the bulk when the colloidal dispersion disorders. The increased structural ordering of the colloidal dispersion near the wall derives from its interaction with its image charge; motion toward the wall is impeded by the motion of the accompanying image charge toward the wall.

B. Negative wall, $\sigma_w<0$

The quartz surface acquires a negative surface potential; the effective surface potential (zeta potential) will depend on the pH of the dispersion.[29] We calculated the pH values of the colloidal crystals at their respective melting impurity concentrations, and determined from the results of Ramachandran and Somasundaram the effective surface potential of the quartz wall. The effective negative bound surface charge density on the wall is obtained using Eq. (15). The charge image from the screening small ion cloud at the container wall also electrostatically interacts with the particle planes. The wall repels the particle plane, while the image charge of the wall screening counterions attracts the particle plane. Thus, in addition to the interplanar and image plane interactions, which occur in the neutral case, an additional negative and positive contribution to the interaction energy of the planes results from the wall and the screening counterion image charge.

The PE curves for the first three planes were calculated using Eqs. (20)–(22) at n_i^m. The results are very similar to those in Fig. 3. The PE curve for the first plane is also distinctly asymmetric about the minimum. These results can be directly compared to the experimental data of Grier and Murray,[18] who examined 325 nm polystyrene spheres with 50 000 titratable charge per sphere in a cell with a negatively charged quartz surface. They found an asymmetric motion of colloidal particles about the equilibrium position of the plane next to the quartz wall. The rms excursion toward the wall was $\sim$0.1 μm from the average distance, while the excursion was 2.5-fold larger away from the wall (0.25 μm).

Our calculated scaled rms displacements, which are listed in Table III, indicate that the first three planes lie farther from melting than the interior planes. On comparing these Δ with those of the neutral wall (Table II), we observe that the stability of the first three planes near the negative wall is less than near the neutral wall. Thus, the negative wall apparently destabilizes the ordering of planes. Increasing the surface negative charge density increases the destabilization. However, Δ_1, Δ_2, Δ_3 are smaller than W_p even for the negative surface. This again indicates that the first plane would melt last during colloidal melting and will order first during crystallization.

Table III shows that $d_1<d_{hkl}$ for systems A, B, and C, whereas $d_1>d_{hkl}$ for system D. For negative surface charged wall, the relative plane spacing depends upon the relative surface charge densities of colloid plane and the quartz wall. This reconciles the different observations in Table III and those of Kesavamoorthy *et al.*,[12] who observed $d_1<d_{hkl}$ and those of Pouligny,[21] who observed $d_1>d_{hkl}$.

Since the first plane is held rigidly as compared to other planes, this plane will order first with a hexagonal 2-D ordering, which minimizes the interaction energy. Thus, hexagonal 2-D ordering has previously been observed in many colloidal dispersions.[10,12–14,17,18]

Systems A, B, and C show that $d_1<d_{hkl}$. Thus, particles in these systems are attracted toward the wall, and the particle concentration near the wall is increased compared to the bulk. This behavior has been experimentally observed in 140

TABLE IV. Calculated parameters for the positive wall.

System	A	B	C	D
n_i^m/n_pZ	1.03	0.94	0.72	1.19
$-\sigma$ (statcoul/cm^2)	233.60	460.00	367.70	50.20
σ_w (statcoul/cm^2)	159.60	258.50	187.70	62.80
$N/10^9$ cm^2	1.702	2.7008	1.654	0.232
d_1/nm	58.00	55.00	62.00	[a]
d_2/nm	206.00	166.00	204.00	[b]
d_3/nm	208.30	168.00	206.00	[b]
d_{hkl}/nm	212.70	168.80	206.70	552.20
Δ_1 %	1.02	1.00	1.01	···
Δ_2 %	4.37	4.30	3.83	···
Δ_3 %	4.70	4.44	3.93	···
W_p %	4.78	4.61	4.07	4.44

[a]The colloid plane collapses onto the quartz wall.
[b]The modeling cannot calculate the spacing if the first colloid plane collapses.

and 245 nm silica particle colloidal dispersions.[13] As n_i is decreased, the 2-D hexagonal ordering will extend to plane 2, then plane 3, and so on. Hence, we obtain a set of stacked 2-D hexagonal planes. After nucleation at the surface, 2-D plane stacking will form a 3-D crystalline ordering.[13] Grier and Murray[18] have reported that the four planes nearest to the wall formed just before the whole suspension freezes. In the present work, we find that three planes nearest to the wall are stabilized more compared to the interior planes.

C. Positive wall, $\sigma_w > 0$

The wall surface can be chemically modified to have a positive surface charge. We considered a positive wall with $|\sigma_w|$ identical to that of the negative wall above and calculated the PE curves of planes 1, 2, and 3 using Eqs. (20)–(22) at n_i^m. Table IV gives the positions of these planes, their Lindemann-type parameter, and other relevant parameters for the colloidal systems. The scaled rms displacements show that the planes near the wall are held more rigidly than in the neutral wall case. The first few planes are strongly attracted toward the wall. In fact calculations for system D predict that the first plane will collapse onto the wall. A positive wall is found to favor the stability of the nearby plane more than the neutral wall. Hence, positively charged surfaces induce the ordering of the colloidal crystal better than the negative or neutral wall.

IV. CONCLUSION

We calculated the effect of a container wall on a colloidal crystalline array by modeling the colloidal crystal as a set of particle planes oriented parallel to the container surface. The charge in the dispersion induces an image charge in the quartz container wall which influences the first layer ordering and spacing. We calculate the colloid charge density on the planes and the interaction energy of the first three planes with the wall, with adjacent colloid planes and with the image charges. The PE curves for first three planes near the wall are computed for cases where the boundary wall charge density is positive, negative, and neutral. These results clearly explain the recent experimental observations of an increased particle concentration near the wall and the formation of 2-D hexagonal layers near the wall prior to formation of 3-D crystals. The scaled rms displacements calculated are less than that for interior colloid. For a neutral wall, the nearest planes to the wall are more stabilized than interior colloid planes. A negative charge on the wall destabilizes the nearest colloid planes; however, they are more stable than the interior planes. The positive wall enhances the stability of the nearest planes more than a neutral or negative wall.

ACKNOWLEDGMENTS

The authors gratefully acknowledge financial support from the Office of Naval Research through Grant No. N00014-94-1-0592 and the National Science Foundation.

[1] W. B. Russel, D. A. Saville, and W. R. Schowalter, *Colloidal Dispersions* (Cambridge University Press, New York, 1988).
[2] M. O. Robbins, K. Kremer, and G. S. Grest, J. Chem. Phys. **88**, 3286 (1988).
[3] R. Kesavamoorthy, A. K. Sood, B. V. R. Tata, and A. K. Arora, J. Phys. C **21**, 4737 (1988).
[4] J. C. Zahorchak, R. Kesavamoorthy, R. D. Coalson, and S. A. Asher, J. Chem. Phys. **96**, 6873 (1992).
[5] P. Pieranski, Contemp. Phys. **24**, 25 (1983).
[6] E. J. W. Verwey and J. Th. G. Overbeek, *Theory of Stability of Lyophobic Colloids* (Elsevier, Amsterdam, 1948).
[7] M. K. Udo and M. F. de Souza, Solid State Commun. **35**, 907 (1980).
[8] H. M. Lindsay and P. M. Chaikin, J. Chem. Phys. **76**, 3774 (1982).
[9] N. Ise, Angew. Chem. Int. Ed. Engl. **25**, 323 (1986).
[10] N. A. Clark, A. J. Hurd, and B. J. Ackerson, Nature (London) **281**, 57 (1979).
[11] S. A. Asher, P. L. Flaugh, and G. Washinger, Appl. Spectrosc. **1**, 26 (1986); S. A. Asher, U.S. Patent Nos. 4,627,689 and 4,632,517.
[12] R. Kesavamoorthy, M. Rajalakshmi, and C. Balu Rao, J. Phys.: Condens. Matter **1**, 7149 (1989).
[13] R. Kesavamoorthy, S. Tandon, S. Xu, S. Jagannathan, and S. A. Asher, J. Colloid Interface Sci. **153**, 188 (1992).
[14] I. S. Sogami and T. Yoshiyama, Phase Transit. **21**, 171 (1990).
[15] Y. Monovoukas and A. P. Gast, J. Colloid Interface Sci. **128**, 533 (1989).
[16] P. A. Rundquist, R. Kesavamoorthy, S. Jagannathan, and S. A. Asher, J. Chem. Phys. **95**, 1249 (1991).
[17] R. Kesavamoorthy, C. Babu Rao, and B. V. R. Tata, J. Phys.: Condens. Matter **3**, 7973 (1991).
[18] D. G. Grier and C. A. Murray, J. Chem. Phys. **100**, 9088 (1991).
[19] A. van Blaaderen and P. Wiltzius, Science **270**, 1177 (1995).
[20] B. V. R. Tata and A. K. Arora, J. Phys.: Condens. Matter **3**, 7983 (1991).
[21] B. Pouligny, D. J. W. Aastuen, and N. A. Clark, Phys. Rev. A **44**, 6616 (1991).
[22] P. A. Gohman, G. Bambakidis, and R. J. Spry, J. Appl. Phys. **67**, 40 (1990).
[23] P. A. Rundquist, S. Jagannathan, R. Kesavamoorthy, C. Brnardic, S. Xu, and S. A. Asher, J. Chem. Phys. **94**, 711 (1991).
[24] R. Kesavamoorthy, S. Jagannathan, P. A. Rundquist, and S. A. Asher, J. Chem. Phys. **94**, 5172 (1991).
[25] S. J. Miklavic, D. Y. C. Chan, L. R. White, and T. W. Healy, J. Phys. Chem. **98**, 9022 (1994).
[26] L. D. Landau, E. M. Lifshitz, and L. P. Pitaenskii, *Electrodynamics of Continous Media*, 2nd ed. (Oxford University Press, New York, 1984).
[27] D. R. Corson and P. Lorrain, *Introduction to Electromagnetic Fields and Waves* (W. H. Freeman, San Francisco, 1962).
[28] R. Ramachandran and P. Somasundaram, Colloids Surf. **21**, 355 (1986).
[29] R. Kesavamoorthy, B. V. R. Tata, A. K. Arora, and A. K. Sood, Phys. Lett. A **138**, 208 (1989).
[30] R. Kesavamoorthy (private communication).
[31] P. A. Rundquist, R. Kesavamoorthy, and S. A. Asher (private communication).
[32] F. A. Lindemann, Z. Phys. **11**, 609 (1910).
[33] K. Kremer, M. O. Robbins, and G. S. Grest, Phys. Rev. Lett. **57**, 2694 (1986).
[34] R. O. Rosenbergh and D. Thirumalai, Phys. Rev. A **36**, 5690 (1987).